Comparative Analysis of the Effectiveness of Intentional Electromagnetic Interference Suppression in Low-Pass Filters

Ye. Zhechev(✉) and A. Zabolotsky

Tomsk State University of Control Systems and Radioelectronics, 40, Prospect Lenina, Tomsk 634050, Russia
zhechev75@gmail.com

Abstract. This paper presents a comparative analysis of three low-pass filter (LPF) structures based on: 1) modal filtering and an electromagnetic absorber (LPF1); 2) a suspended substrate with a double-sided pattern of strip conductors (LPF2); and 3) a two-dimensional microstrip electromagnetic crystal (LPF3). The effectiveness of each filter in suppressing ultrawideband (UWB) and narrowband (NB) electromagnetic interference (EMI) is evaluated. Frequency and time domain characteristics of the filters are obtained using the finite-difference time-domain (FDTD) and finite element (FEM) methods. N-norms and eye diagrams are analyzed to comprehensively assess EMI attenuation and its impact on signal integrity. The results show that LPF1 exhibits a smaller passband compared to LPF2 and LPF3. However, despite significantly smaller dimensions, LPF1 demonstrates the highest attenuation coefficient for both UWB and NB EMI in the time domain. In terms of signal integrity, LPF1 shows superior performance at data rates up to 2 Gbps due to its stable group delay values in the frequency range from 0 to 2.2 GHz.

Keywords: Low-pass filter · Electromagnetic absorber · Electromagnetic compatibility · Signal integrity

1 Introduction

Modern radio-electronic devices (REDs) are increasingly reliant on sophisticated electronic systems to achieve high levels of automation. This trend towards complex electronics, while offering numerous advantages, also introduces a significant vulnerability to various electromagnetic influences [1]. Advancements in the generation of high-power electromagnetic pulses and radio frequency radiation have led to the development of systems and devices capable of disrupting the functionality of REDs, posing a significant threat to their reliability and safety [2–6].

Traditionally, the field of radio engineering has addressed the problem of electromagnetic interference (EMI) mitigation through linear filtering, employing linear frequency filters. These filters were typically designed to provide a maximally flat passband for the desired signal and maximum suppression of frequencies outside this band. An ideal

A. A. Radionov and V. R. Gasiyarov (Eds.): RusAutoCon 2024, LNEE 1324, pp. 375–386, 2025.
https://doi.org/10.1007/978-3-031-82494-4_33

filter was considered to have a rectangular amplitude-frequency response (AFR), effectively eliminating all unwanted frequencies while allowing the desired signal to pass unimpeded.

However, with the development of information theory and statistical signal detection theory, it became evident that this approach has significant limitations. The conventional linear filtering approach fails to account for the specific waveform of the desired signal and the statistical properties of EMI. Consequently, a filter with a rectangular AFR is not optimal when a priori information about the signal waveform and EMI characteristics is available [7]. Furthermore, these filters exhibit a reflection coefficient (S_{11}) close to unity in their stopband. When integrated into complex radio-electronic systems with multiple frequency channels, these filters can cause reflections that lead to undesirable electromagnetic interactions between system elements, potentially compromising the overall system performance [8].

To address these limitations, absorptive filters, such as those based on modal filtering, have been proposed [8, 9]. These filters achieve EMI suppression by separating the EMI pulse in time due to the difference in propagation speeds of the fundamental modes in the filter structure. In their stopband, such filters typically exhibit a low S_{11} value, minimizing unwanted reflections. However, the large size of modal filters has historically hindered their application in modern REDs, where space constraints are often paramount.

To overcome the size limitations while preserving the effectiveness of modal filtering, a novel approach has emerged: combining modal filtering with electromagnetic absorbers. These absorbers are characterized by high relative permittivity and permeability (ε_r and μ_r) and high dielectric and magnetic loss tangents ($tg\delta_\varepsilon$ and $tg\delta_\mu$) [10]. A compact filter utilizing modal filtering, an electromagnetic absorber, and a meander conductor routing scheme from [11] with strong coupling was presented in [12]. This filter demonstrated promise as a low-pass filter (LPF) with a wide stopband. However, the published results did not definitively showcase the advantages of this combined approach.

Therefore, this paper aims to analyze the effectiveness of suppressing ultrawideband (UWB) and narrowband (NB) EMI in conventional and proposed LPFs to evaluate the potential benefits of this novel approach. We compare the performance of the proposed LPF with two well-known LPF designs, highlighting its advantages in terms of EMI suppression, size, and signal integrity. By providing a comprehensive comparison of these filter structures, this study seeks to contribute to the development of more effective and compact EMI mitigation solutions for modern REDs.

2 Structures, Approaches, and Methods

This section describes the structures of the three LPFs under investigation, the methods employed for analysis, and the types of interference signals used to evaluate their performance.

Three different LPF structures are investigated in this study:

1. LPF1: This filter utilizes a combination of modal filtering and an electromagnetic absorber, as detailed in [11]. To improve its passband, the length (l) of the regular part of the active conductor was reduced from 200 to 50 mm, while other parameters

remained identical to the original prototype ($w = 200$ μm, $s = 400$ μm, $d = 200$ μm, $h = 250$ μm, $h_1 = 500$ μm, $t = 18$ μm, $\varepsilon_{r1} = 4.6$, $tg\delta_1 = 0.018$). The principle of operation of LPF1 is based on modal filtering, which utilizes the difference in propagation velocities of various modes in the structure. To achieve strong modal distortions, a second conductor (P) is traced alongside the signal conductor (A), as shown in Fig. 1(a). Conductor A is connected to a voltage source E with internal resistance R_s at its near end and to a load R_l at its far end. The beginning and end of conductor P are connected to the circuit ground through resistors R. All resistances are set to 50 Ω. An electromagnetic absorber is placed on top of the conductor P, as shown in Fig. 1(b).

2. LPF2: This filter utilizes a suspended substrate with a double-sided pattern of strip conductors, as described in [13].
3. LPF3: This filter is based on a two-dimensional microstrip electromagnetic crystal, as presented in [14].

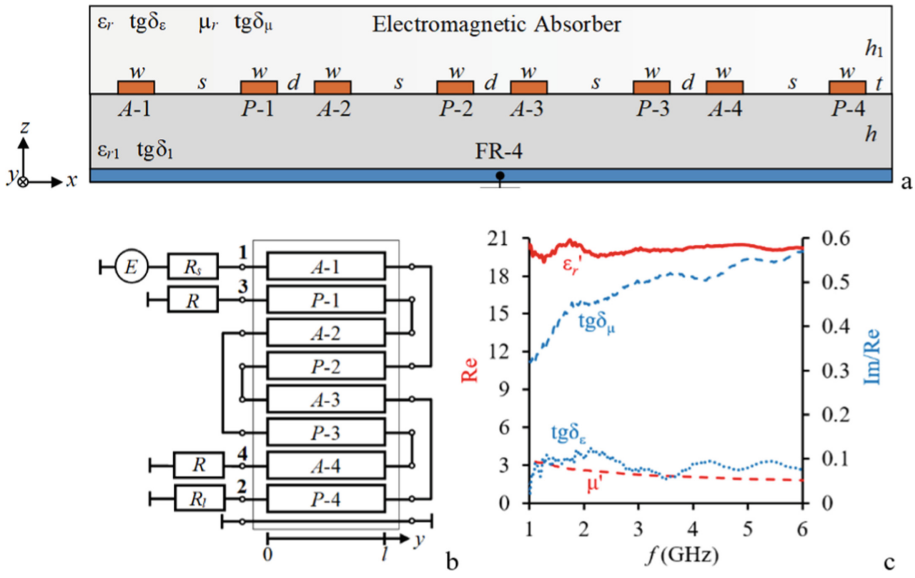

Fig. 1. (a) Cross-section of the regular part of LPF1, (b) its connection diagram and (c) parameters of the electromagnetic absorber.

The selection of LPF2 and LPF3 for comparison is based on their high steepness and significant suppression (up to 100 dB) in the stopband. Notably, LPF1, with a PCB size of 8x15x0.25 (mm), is considerably smaller than its counterparts 24.4x60x1 (mm) for LPF2 and 9x53x0.5 (mm) for LPF3, as shown in Fig. 2.

The frequency and time domain characteristics of the LPFs were analyzed using an electrodynamic approach with the finite-difference time-domain (FDTD) and finite element (FEM) methods. The geometry and electrophysical parameters of the reference filters were obtained from their respective publications. Their modeling was performed

considering dielectric losses ($\tan\delta = 0.0001$) and conductor losses ($\sigma = 5.96 \cdot 10^7$ S/m). The frequency analysis was carried out in the range from 0 to 20 GHz. After characterizing the devices in the frequency domain, a time-domain response analysis was performed.

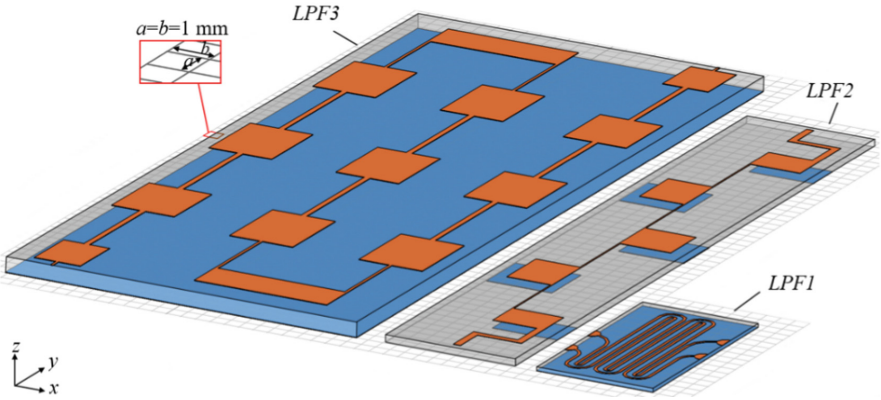

Fig. 2. Structures of the devices under study.

The input of the investigated filters was subjected to pulses corresponding to UWB (Fig. 3) and NB (Fig. 4) EMI according to IEC standard for electromagnetic compatibility. To comprehensively assess EMI attenuation, N-norms were analyzed. *N*-norms are mathematical operators used to describe the impact of specific destabilizing EMI factors on RED components [15]. The expressions used to calculate the *N*-norms are presented in Table 1. In the results section, the output *N*-norm values are normalized to half of the electromotive force (EMF), simulating the case without any filters.

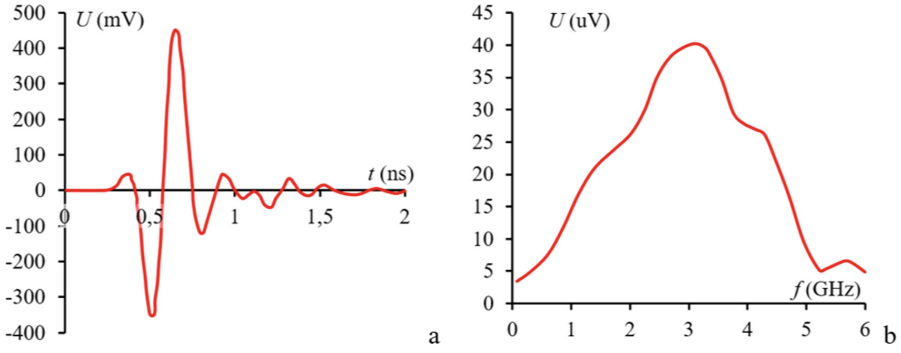

Fig. 3. UWB EMI pulse: (a) voltage waveform and (b) spectrum.

To evaluate signal integrity, group delay time (GDT) was analyzed in the frequency range from 0 to 2.2 GHz. Additionally, eye diagrams were analyzed, obtained using a pseudorandom bit sequence source (with an EMF amplitude of 1 V) connected to the

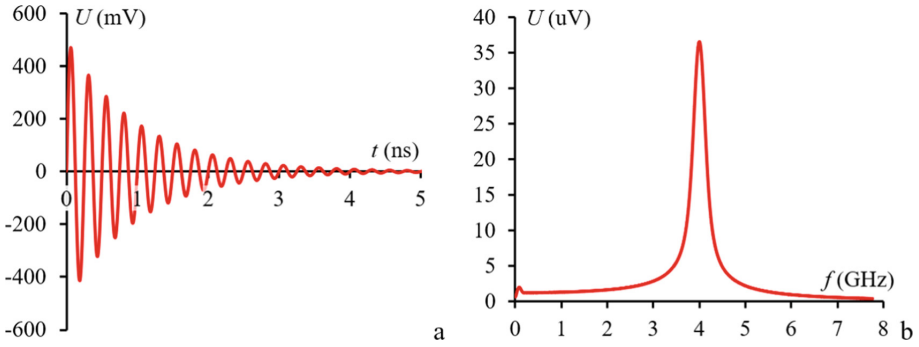

Fig. 4. NB EMI pulse: (a) voltage waveform and (b) spectrum.

investigated devices. Two data rates were used: 1 and 2 Gbps (with rise/fall times of 100 and 50 ps, respectively). Their choice is determined by the bandwidth of the reference filters.

Table 1. The brief explanation of the *N*-norms.

No	N_1	N_2	N_3	N_4	N_5
Equation	$\|U(t)\|_{\max}$	$\left\|\frac{\delta U(t)}{\delta t}\right\|$	$\left\|\int_0^t U(t)\right\|_{max}$	$\int_0^\infty \|U(t)\|dt$	$\left\{\int_0^\infty \|U(t)\|^2 dt\right\}^2$
Name	Peak value (absolute)	Peak value (absolute)	Peak value (absolute)	Peak value (absolute)	Peak value (absolute)
Failures	Circuit upset/ electric breakdown/ arc-over effects	Circuit upset/ electric breakdown/ arc-over effects	Circuit upset/ electric breakdown/ arc-over effects	Circuit upset/ electric breakdown/ arc-over effects	Circuit upset/ electric breakdown/ arc-over effects

3 EMI Suppression

This section presents the frequency and time-domain characteristics of the investigated LPFs, providing insights into their effectiveness in suppressing UWB and NB EMI. The frequency responses, obtained through both FDTD and FEM simulations, highlight the filter's passband and stopband characteristics, revealing the cutoff frequencies and suppression levels achieved by each filter. Furthermore, the time-domain responses to both UWB and NB EMI pulses are analyzed to assess the filters' ability to attenuate the amplitude and duration of these interference signals. This analysis provides a detailed understanding of how each LPF structure interacts with different types of EMI and its impact on signal integrity.

The frequency dependences of the investigated LPFs obtained by the two methods are presented in Fig. 5. From the point of view of $|S_{11}|$, it can be seen that all devices are matched in the passband, with the lowest values obtained for LPF2. From these characteristics, it can be seen that the LPF1 weakly reflects the interference in the entire frequency range under study. From the characteristic $|S_{21}|$, it can be seen that the cutoff frequencies are 0.57 GHz for LPF1, 1.87 GHz for LPF2, and 2.26 GHz for LPF3. Consequently, the suppression ratio of different EMI will be different. It can also be seen that LPF2 and LPF3 have significant suppression in some frequency range after the passband. However, their complex EMI suppression efficiency at high frequencies is significantly reduced, which may be attributed to the topology and design of these filters. At the same time, LPF1 has stable suppression (35 dB) in the range from 5 to 20 GHz.

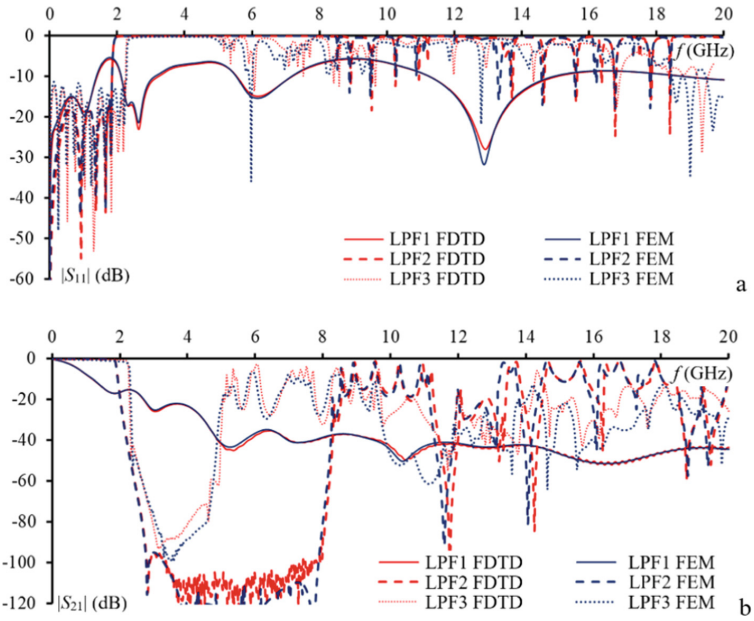

Fig. 5. Frequency dependences of (a) $|S_{11}|$ and (b) $|S_{21}|$ of the investigated LPFs obtained by two methods.

Figures 6 and 7 illustrate the responses to UWB and NB EMI, respectively. Given the broad spectrum and complex shape of real EMI [16, 17], the barrier bandwidth exerts a greater influence on the output response than the maximum suppression. The suppression of the analog filters in the low and high frequency regions is insignificant, resulting in the maximum amplitude of the output voltage. In the case of LPF3, there are also high-frequency components in the response, which can be explained by examining the graph of frequency dependence $|S_{21}|$. In the case of LPF1, the highest attenuation is observed in the high frequency region (above 5 GHz). However, due to the greater attenuation of EMI amplitude in the range from 0 to 2.5 GHz, this filter exhibits the highest attenuation coefficient of UWB and NB interference among the investigated

LPFs. It appears that as the center frequency of NB EMI increases, their suppression by the filter-analogues will worsen.

From the perspective of N-norms, it can be observed that LPF1 has the capacity to significantly attenuate N_1, N_2, N_4 and N_5 (Tables 2 and 3). Furthermore, the proposed filter demonstrates a greater degree of attenuation of N_1, N_4 and N_5 than the counterpart filters. The notable increase in N_3 for NB EMI can be attributed to the fact that all considered devices introduce significant distortion to the voltage waveform. Consequently, the absolute small value of this norm increases. Nevertheless, due to the very small value of N_3, this norm can be neglected.

Table 2. Normalized N-norms for the UWB EMI.

Voltage waveform	N_1	N_2	N_3	N_4	N_5
EMF/2	1	1	1	1	1
LPF1 FDTD	0.117	0.068	1.000	0.215	0.138
LPF1 FEM	0.122	0.070	1.000	0.226	0.141
LPF2 FDTD	0.165	0.066	1.000	0.978	0.325
LPF2 FEM	0.163	0.065	1.000	0.968	0.325
LPF3 FDTD	0.196	0.113	1.000	1.656	0.431
LPF3 FEM	0.202	0.106	1.000	1.409	0.400

4 Signal Integrity

This section examines the impact of the investigated LPFs on signal integrity, focusing on their ability to maintain the quality of data transmission under different conditions. The frequency dependence of the GDT is analyzed to assess the filters' distortion introduced to the useful signal. Additionally, eye diagrams generated using a pseudorandom bit sequence at 1 and 2 Gbps provide visual insights into the filters' effect on data transmission and their suitability for different data rates. This analysis aims to identify the filter that exhibits the most stable signal transmission characteristics, minimizing distortion and ensuring high-quality data transmission.

Figure 8 illustrates the frequency dependence of GDT. The graph indicates that within the range of 0 to 2.2 GHz, the proposed filter exhibits the most consistent response (0.81 ns $\pm$ 0.115 ns). In contrast, LPF2 exhibits values of 1.06 ns $\pm$ 0.56 ns, and LPF3 exhibits values of 2.47 ns $\pm$ 1.06 ns. The instability of the GDT of the analog filters explains why, despite the smaller bandwidth of LPF1, it introduces less distortion to the useful signal. Since it is demonstrated in the paper that the results obtained by the two types of modeling agree well with each other, the eye diagrams obtained with FDTD alone are presented below (Fig. 9). The signal parameters are summarized in Table 4.

The eye diagrams in Fig. 9 provide visual confirmation of these observations. At a data rate of 1 Gbps, LPF1 demonstrates the most desirable performance. It exhibits

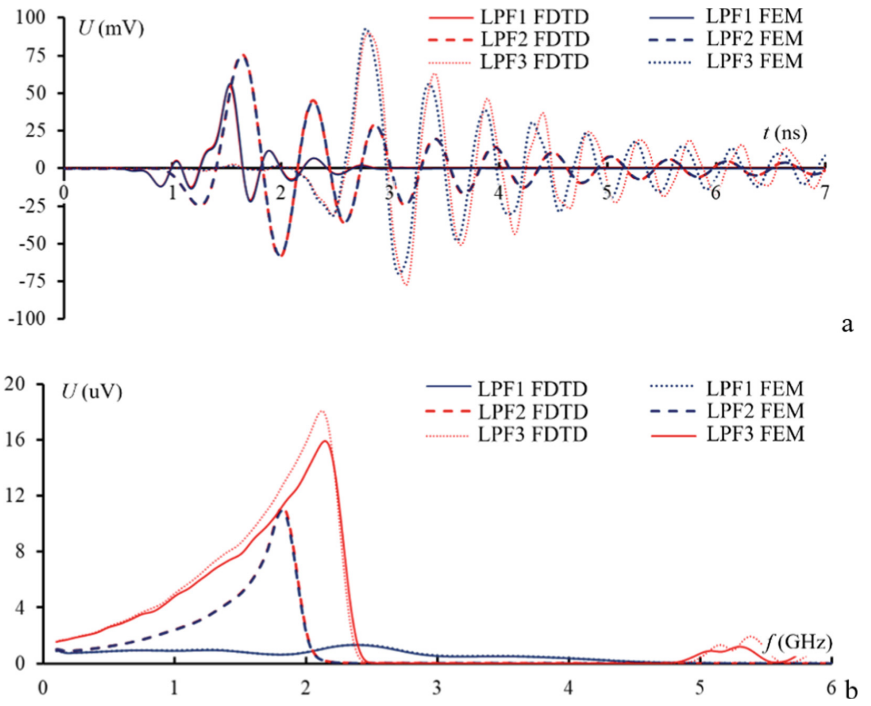

Fig. 6. Responses to the UWB EMI pulse: (a) output voltage waveforms and (b) their spectrum.

the highest signal-to-noise ratio and the lowest phase deviation, as evidenced by the clear, well-defined transition between logic zero and one levels. This suggests that LPF1 introduces minimal distortion to the useful signal at this data rate. While the counterpart filters (LPF2 and LPF3) also exhibit acceptable levels of distortion, they are demonstrably inferior to LPF1 in terms of signal integrity at 1 Gbps.

As the data rate is increased to 2 Gbps, a noticeable deterioration in the signal-to-noise ratio, phase deviation, and eye-opening degree is observed for all LPFs. This is to be expected, as the increased data rate demands faster switching speeds, potentially exacerbating the effects of parasitic capacitance and inductance in the filter structures. Despite this degradation, all filters still maintain a functional eye opening, indicating that they could be utilized in radio circuits requiring high data rates. However, it is crucial to note that the eye opening for LPF1 is the most affected by the higher data rate, exhibiting a significant decrease in clarity. However, it is important to note that despite the narrower eye opening, LPF1 maintains a stable and consistent voltage level, without any noticeable fluctuations in the upper and lower logic levels. This stability is crucial for reliable data transmission and suggests that LPF1 can still function effectively at 2 Gbps, even if with slightly lower performance compared to 1 Gbps.

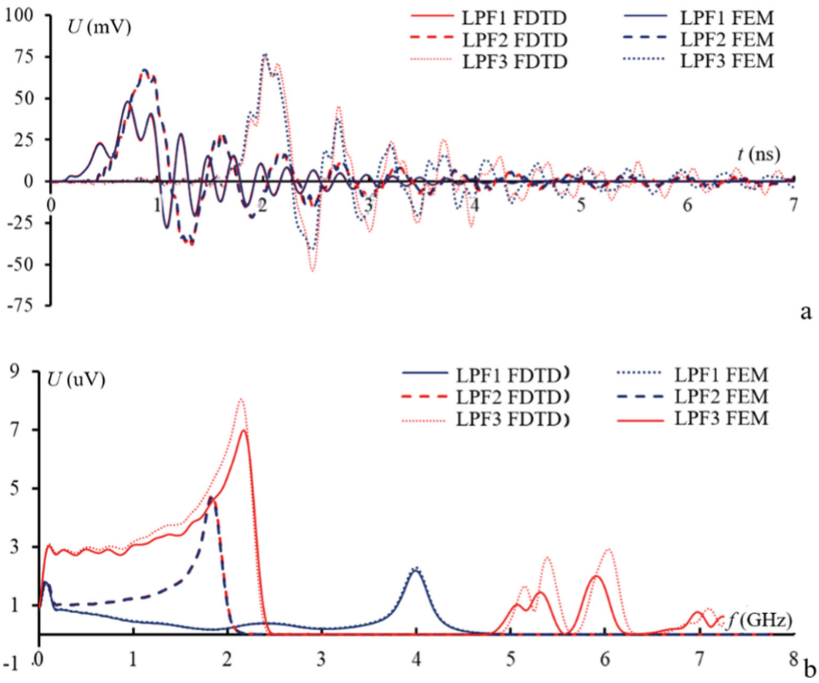

Fig. 7. Responses to the NB EMI pulse: (a) output voltage waveforms and (b) their spectrum.

Table 3. Normalized N-norms for the NB EMI.

Voltage waveform	N_1	N_2	N_3	N_4	N_5
EMF/2	1	1	1	1	1
LPF1 FDTD	0.102	0.057	12.532	0.116	0.116
LPF1 FEM	0.102	0.059	12.532	0.119	0.112
LPF2 FDTD	0.145	0.055	12.532	0.200	0.168
LPF2 FEM	0.143	0.058	12.532	0.197	0.164
LPF3 FDTD	0.162	0.070	12.532	0.288	0.192
LPF3 FEM	0.164	0.067	12.532	0.241	0.180

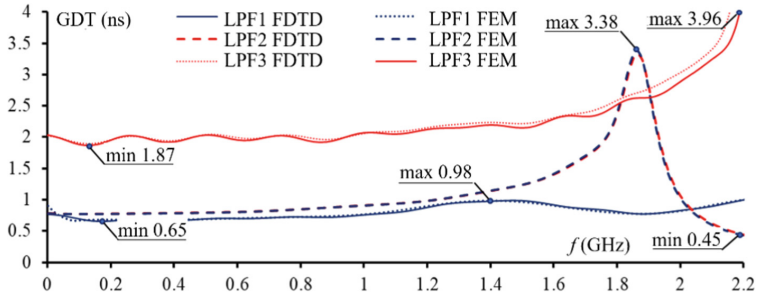

Fig. 8. Frequency dependences of GDT.

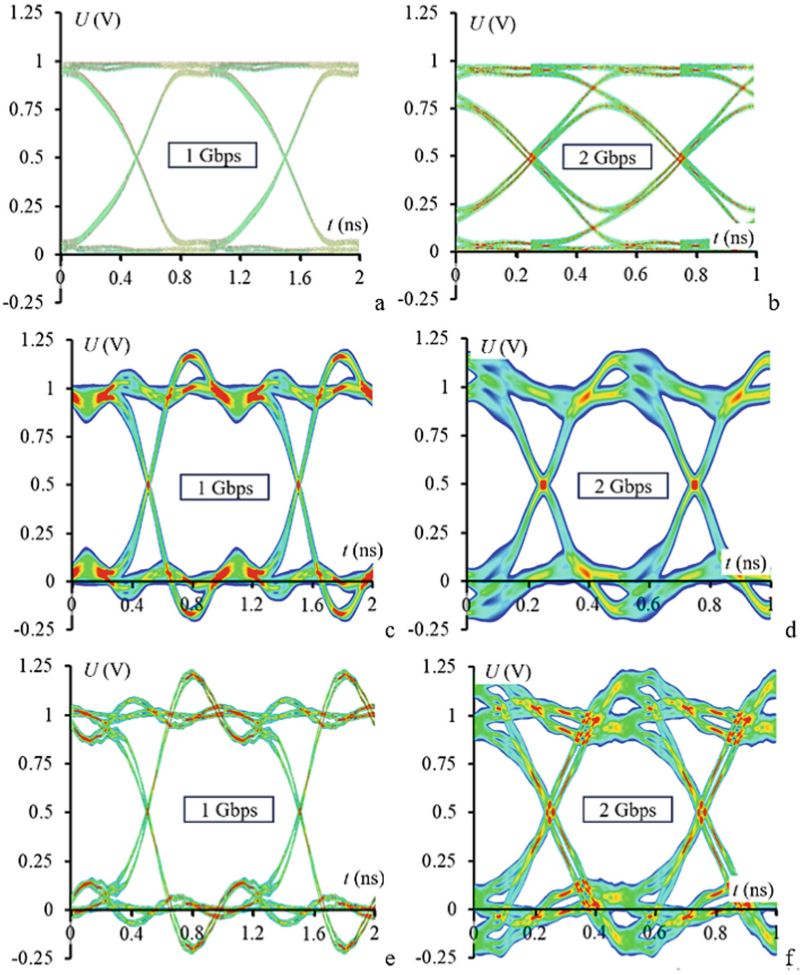

Fig. 9. Eye diagrams obtained by FDTD: (a), (b) for LPF1; (c), (d) for LPF2; (e), (f) for LPF3.

Table 4. Parameters of the pseudo-random bit sequence.

Parameter	Ca	LPF1		LPF2		LPF3	
		FDTD	FEM	FDTD	FEM	FDTD	FEM
Eye height	1	0.82	0.81	0.66	0.67	0.75	0.76
	2	0.47	0.48	0.95	0.95	0.93	0.94
Eye width	1	0.96	0.96	0.44	0.43	0.41	0.42
	2	0.43	0.42	9.76	9.81	9.81	9.32
Jitter RMS	1	2.7	3.5	12.3	12.3	12.6	11.6
	2	8.1	7.6	8.17	9.2	9.69	10.9
Signal-to-noise ratio	1	21.7	22.3	4.99	5	6.77	8.38
	2	4.52	4.6	0.71	0.70	0.61	0.67

5 Conclusion

This section examines the suppression efficiency of UWB and NB EMI in three different LPFs. Analysis of frequency characteristics reveals that LPF1 possesses a narrower bandwidth (0.57 GHz) and lower maximum suppression in the stopband (51 dB) compared to LPF2 (1.87 GHz; 120 dB) and LPF3 (2.26 GHz; 100 dB). The design of the printed circuit boards and the conductor topology of LPF2 and LPF3 result in a decrease in their suppression of EMI at higher frequencies. In contrast, LPF1 exhibits consistent suppression across the entire frequency range under investigation. The lower values of $|S_{11}|$ observed for LPF1, including in the stopband, make it particularly well-suited for use in systems requiring complex frequency separation of channels.

The N-norms analysis confirms that LPF1 provides the highest attenuation for both UWB and NB EMI. This superior performance is attributed to the wider bandwidth of LPF2 and LPF3, as well as the presence of parasitic electromagnetic coupling at higher frequencies in these filters. For UWB EMI (FDTD), LPF1 demonstrates an attenuation of N_1 by 8.19 times, N_2 by 14.7 times, and N_5 by 7.24 times, exceeding the attenuation achieved by LPF2 and LPF3. Similar attenuation patterns are observed for NB EMI, with the center frequency of LPF2 and LPF3 aligning with their maximum suppression regions.

Signal integrity analysis demonstrates that LPF1 performs best for a data rate of 1 Gbps, due to its stable GDT values in the frequency range from 0 to 2.2 GHz. However, increasing the data rate to 2 Gbps leads to distortion in the useful signal waveform for all filters. LPF2 and LPF3 exhibit a more open "eye" at 2 Gbps, but with significant phase and amplitude variations.

Acknowledgments. The research was supported by the Russian Science Foundation under Project No. 23-29-00486 (https://rscf.ru/en/project/23-29-00486/) at TUSUR.

References

1. Gonorovskii, I.: Radio engineering circuits and signals. Sovetskoe Radio, Moscow (1977)
2. Gaynutdinov, R.R., Chermoshentsev, S.F.: Electromagnetic Interference emission from communication lines of onboard equipment of an unmanned aerial vehicle. J. Commun. Technol. Electron. **65**, 221–227 (2020). https://doi.org/10.1134/S1064226920020059
3. Bystrov, R.P., Potapov, A.A., Cherepenin, V.A., Dmitriev, V.G., Perunov, Y.M.: Electromagnetic systems and means of deliberate impact on physical and biological objects. J. Radioelectronics. Nanosystems. Inf. Technol. **6**, 129–169 (2014). https://doi.org/10.17725/RENSITe.0006.201412a.0129
4. Kubyshkin, A.V., Belokon, I.N., Stepanov, V.M.: Development of directed energy weapon technologies abroad. Technol. Electromagn. Compat. **77**, 44–55 (2021)
5. Tyo, J.S., Abdalla, M.D., Skipper, M.C.: Differentially fed high-power microwave antennas using capacitively coupled hyperband inverters. IEEE Trans. Antennas Propag. **67**, 5203–5211 (2019). https://doi.org/10.1109/TAP.2019.2917473
6. Bokhan, P.A., Gugin, D.E., Zakrevsky, D.E., Lavrukhin, M.A.: Generation of high-voltage pulses with a picosecond front in a cascade kivotron connection. Instrum. Exp. Tech. **61**, 491–495 (2018). https://doi.org/10.1134/S0020441218030181
7. Podgorski, A.S.: High power microwave weapon. US Patent 10,451,388 (22 Oct 2019)
8. Steer, M.: Fundamentals of microwave and RF design, 3rd edn. North Carolina State University, NC (2019)
9. Sagiyeva, I.Y., Zhechev, Y.S., Kenzhegulova, Z.M., Surovtsev, R.S., Gazizov, T.R.: Modal filter based on a microstrip line with two side conductors grounded at both ends. IEEE Trans. Electromagn. Compat. **65**, 1371–1378 (2019). https://doi.org/10.1109/TEMC.2023.3275388
10. Samoylichenko, M.A., Gazizov, T.R.: Modified microstrip line which can protect against ultrashort pulse. Systems of Control, Communication and Security, 203–214 (2019). https://doi.org/10.24411/2410-9916-2019-10210
11. Zhechev, Y.S., Adnan, A.H., Malygin, K.P.: New technique for improving modal filter performance by using an electromagnetic absorber. IEEE Access **10**, 86663–86670 (2022). https://doi.org/10.1109/ACCESS.2022.3199360
12. Zhechev, Y.S., Murmansky, M.S., Vlasov, S.V., Trubcheninov, V.A., Kuzmin, N.O., Pavlov, N.S.: High-efficiency low-pass reflectionless filter based on modal decomposition and electromagnetic absorber. IEEE Trans. Compon. Packag. Manuf. Technol. **14**, 938–944 (2024). https://doi.org/10.1109/TCPMT.2024.3383840
13. Zhechev, Y.S., Belousov, A.O., Zabolotsky, A.M., Vlasov, S.V., Murmansky, M.S., Pavlov, N.S.: Routing technique for microwave transmission lines to ensure uwb interference immunity. IEEE Trans. Microw. Theory Tech. **71**, 5304–5316 (2023). https://doi.org/10.1109/TMTT.2023.3276029
14. Belyaev, B.A., Serzhantov, A.M., Leksikov, A.A., Balva, Y.F., Grushevskii, E.O., Khodenkov, S.A.: A highly selective stripline lowpass filter with more than 100-dB wide stopband attenuation. Tech. Phys. Lett. **46**, 364–367 (2020). https://doi.org/10.1134/S1063785020040173
15. Belyaev, B.A., Khodenkov, S.A., Galeev, R.G., Shabanov, V.F.: A lowpass filter based on a 2D microstrip electromagnetic crystal. Dokl. Phys. **64**, 85–89 (2019). https://doi.org/10.1134/S1028335819030017
16. Giri, D.V.: High-power electromagnetic radiators: nonlethal weapons and other applications. Harvard University Press, Cambridge, Massachusetts, and London (2004)
17. Mora, N., Vega, F., Lugrin, G., Rachidi, F.: Study and classification of potential IEMI sources. Syst. Des. Ass. Notes **41**, 1–93 (2014)